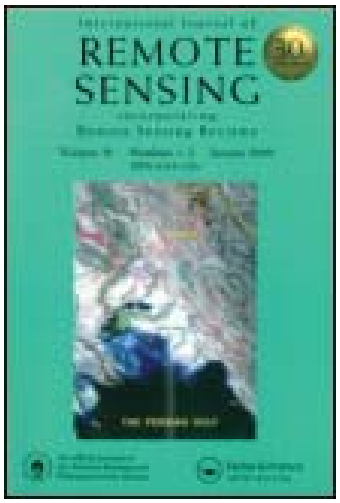

International Journal of Remote Sensing

Publication details, including instructions for authors and subscription information:
http://www.tandfonline.com/loi/tres20

Mapping impervious surface expansion using medium-resolution satellite image time series: a case study in the Yangtze River Delta, China

Feng Gao [a] , Eric Brown de Colstoun [b] , Ronghua Ma [c] , Qihao Weng [d] , Jeffrey G. Masek [b] , Jin Chen [e] , Yaozhong Pan [e] & Conghe Song [f]

[a] Hydrology and Remote Sensing Laboratory, Agricultural Research Service, US Department of Agriculture, Beltsville, MD, 20705, USA

[b] Biospheric Sciences Laboratory, NASA Goddard Space Flight Center, Greenbelt, MD, 20771, USA

[c] Nanjing Institute of Geography & Limnology, Chinese Academy of Sciences, Nanjing, 210008, China

[d] Department of Earth & Environmental Systems, Indiana State University, Terre Haute, IN, 47809, USA

[e] State Key Laboratory of Earth Surface Processes and Resource Ecology, Beijing Normal University, Beijing, 100875, China

[f] Department of Geography, University of North Carolina at Chapel Hill, Chapel Hill, NC, 27599, USA

Version of record first published: 02 Jul 2012

To cite this article: Feng Gao, Eric Brown de Colstoun, Ronghua Ma, Qihao Weng, Jeffrey G. Masek, Jin Chen, Yaozhong Pan & Conghe Song (2012): Mapping impervious surface expansion using medium-resolution satellite image time series: a case study in the Yangtze River Delta, China, International Journal of Remote Sensing, 33:24, 7609-7628

To link to this article: http://dx.doi.org/10.1080/01431161.2012.700424

International Journal of Remote Sensing
Vol. 33, No. 24, 20 December 2012, 7609–7628

Mapping impervious surface expansion using medium-resolution satellite image time series: a case study in the Yangtze River Delta, China

FENG GAO†, ERIC BROWN DE COLSTOUN‡, RONGHUA MA§, QIHAO WENG¶, JEFFREY G. MASEK‡, JIN CHEN|, YAOZHONG PAN| and CONGHE SONG*††

†Hydrology and Remote Sensing Laboratory, Agricultural Research Service, US Department of Agriculture, Beltsville, MD 20705, USA
‡Biospheric Sciences Laboratory, NASA Goddard Space Flight Center, Greenbelt, MD 20771, USA
§Nanjing Institute of Geography & Limnology, Chinese Academy of Sciences, Nanjing 210008, China
¶Department of Earth & Environmental Systems, Indiana State University, Terre Haute, IN 47809, USA
|State Key Laboratory of Earth Surface Processes and Resource Ecology, Beijing Normal University, Beijing 100875, China
††Department of Geography, University of North Carolina at Chapel Hill, Chapel Hill, NC 27599, USA

(*Received 22 October 2011; in final form 15 May 2012*)

Cities have been expanding rapidly worldwide, especially over the past few decades. Mapping the dynamic expansion of impervious surface in both space and time is essential for an improved understanding of the urbanization process, land-cover and land-use change, and their impacts on the environment. Landsat and other medium-resolution satellites provide the necessary spatial details and temporal frequency for mapping impervious surface expansion over the past four decades. Since the US Geological Survey opened the historical record of the Landsat image archive for free access in 2008, the decades-old bottleneck of data limitation has gone. Remote-sensing scientists are now rich with data, and the challenge is how to make best use of this precious resource. In this article, we develop an efficient algorithm to map the continuous expansion of impervious surface using a time series of four decades of medium-resolution satellite images. The algorithm is based on a supervised classification of the time-series image stack using a decision tree. Each imerpervious class represents urbanization starting in a different image. The algorithm also allows us to remove inconsistent training samples because impervious expansion is not reversible during the study period. The objective is to extract a time series of complete and consistent impervious surface maps from a corresponding times series of images collected from multiple sensors, and with a minimal amount of image preprocessing effort. The approach was tested in the lower Yangtze River Delta region, one of the fastest urban growth areas in China. Results from nearly four decades of medium-resolution satellite data from the Landsat Multispectral Scanner (MSS), Thematic

*Corresponding author. Email: csong@email.unc.edu

International Journal of Remote Sensing
ISSN 0143-1161 print/ISSN 1366-5901 online © 2012 Taylor & Francis
http://www.tandfonline.com
http://dx.doi.org/10.1080/01431161.2012.700424

Mapper (TM), Enhanced Thematic Mapper plus (ETM+) and China–Brazil Earth Resources Satellite (CBERS) show a consistent urbanization process that is consistent with economic development plans and policies. The time-series impervious spatial extent maps derived from this study agree well with an existing urban extent polygon data set that was previously developed independently. The overall mapping accuracy was estimated at about 92.5% with 3% commission error and 12% omission error for the impervious type from all images regardless of image quality and initial spatial resolution.

1. Introduction

Due to the rapid growth of population and economic development, more people are now living in cities than in rural areas for the first time in human history (United Nations, 2008). As a result, cities are sprawling rapidly into their surroundings (Seto *et al*. 2002, Schneider *et al*. 2005, Seto *et al*. 2010). This is particularly true for China because of its large population and the rapid economic growth over the past 30 years (Ji *et al*. 2001, Liu *et al*. 2005). China's urban population increased from 20% in 1982 to 46% in 2010 (Peng 2011). Urban environments support an improved quality of life for most of their inhabitants. One may also see urbanization as advantageous to industrial growth and commercial activity. However, excessive expansion of impervious surface can cause a series of environmental problems, including but not limited to loss of habitats for wildlife (McKinney 2002), change of regional climate and water cycles (Zhou *et al*. 2004), loss of fertile land for food production (Seto *et al*. 2002) and altering ecosystem goods and services (Groffman *et al*. 2003, Grimm *et al*. 2008). These impacts have been recognized and studied for decades (Kalnay and Cai 2003), but a complete understanding has been hindered by a lack of consistent geospatial data on global urbanization. Clearly, self-consistent and continuous time-series maps of impervious surface are needed for this effort over any geographic area concerned. A time series of impervious surface maps also provides independent information for decision-makers to monitor land-use and land-cover changes, to evaluate the implementation of land-use policy (Netzband *et al*. 2007) and also to potentially model the future expansion of cities (Herold *et al*. 2003, Jantz *et al*. 2005).

A characteristic change associated with urbanization is the expansion of impervious surface. Satellite remote sensing provides the only viable option to detect and monitor impervious surface from space in an efficient, affordable and timely manner. There are numerous satellite products that offer the potential to monitor urban growth. The night-time lights of the world product derived from the Defense Meteorological Satellite Program (DMSP) Operational Linescan System (OLS) was used to produce the global urban data set at 1 km × 1 km spatial resolution (Elvidge *et al*. 1997, Imhoff *et al*. 1997). Moderate Resolution Imaging Spectroradiometer (MODIS) land-cover products were combined with DMSP nightlight and population data to produce a synergized 1 km × 1 km spatial resolution global urban map (Friedl *et al*. 2002, Schneider *et al*. 2003). Global urban maps at coarse resolution can cover large areas and be updated frequently. However, due to the complex nature of urban landscapes and inherent resolution of human activity, global urban maps at the coarse spatial resolution have been difficult to use within many applications and for policy makers at local to regional scales (Small 2003). This is also due to their limited mapping accuracy and difficulty in accurately describing finer resolution objects such as roads, buildings and other infrastructure.

Medium-resolution optical satellite imagery possesses unique advantages in mapping urban areas accurately and over time. It provides the detailed information with sufficient spatial and temporal resolution for detecting urban expansion. Sensors onboard the Landsat series of satellites, including the Multi-Spectral Scanner (MSS), Thematic Mapper (TM) and Enhanced Thematic Mapper plus (ETM+), have been providing Earth observation data continuously since the early 1970s and form the cornerstone for medium-resolution remote sensing (Townshend *et al*. 1991, Loveland and Shaw 1996). Many urbanization mapping activities at local, regional and continental scales have been conducted at this spatial resolution (Seto *et al*. 2000, 2002, Jantz *et al*. 2005, Schneider *et al*. 2005). As part of the National Land Cover Dataset (NLCD), impervious surface maps were produced for the USA from Landsat data for the first time (Homer *et al*. 2004). Data from Landsat have also been used successfully in land-use and land-cover change detection (Gutman *et al*. 2004). However, the majority of urban land-cover and land-use studies have tended to focus on a single image at one time in the past (Schneider *et al*. 2003, Wu and Murray 2003, Song 2005). Applications using Landsat data are surging thanks to the availability of free Landsat data from the US Geological Survey (http://glovis.usgs.gov/) since 2008 (Woodcock *et al*. 2008). Therefore, approaches that take advantage of the moderate-resolution image time series and produce consistent maps for urban expansion will be highly valuable for urban ecologists, city and regional planners and remote-sensing scientists monitoring land-cover/land-use changes. These data sets would also allow for more detailed studies to determine the impact or consequences of such changes on the water, carbon and energy cycles, and even climate.

Continuity of medium-resolution (or Landsat-like) data is critical for monitoring land-cover/land-use change. However, the failure of the Scan-Line Corrector (SLC) onboard the Landsat 7 satellite in 2003 caused a loss of ~25% of the data toward the edges of each image, and Landsat 5 suspended operations in November 2011. Although the new Landsat Data Continuity Mission (LDCM) satellite is expected in orbit in early 2013, maintaining the continuity of Landsat style medium-resolution remotely sensed data is precarious. This situation highlights the need to combine the capabilities of existing international sensors to provide a more robust observational record. The China–Brazil Earth Resources Satellite-2 (CBERS-2) was launched on 21 October 2003. It has a similar satellite orbit (778 km) and equatorial crossing time (at local time 10:30 am) as Landsat and carries the Charge Coupled Device (CCD) and Infrared MultiSpectral Scanner (IRMSS) cameras (Wang *et al.* 2000, Sausen 2001). The CCD visible and NIR bandwidths are almost identical to Landsat but with a 20 m spatial resolution. It is a valuable source of data to integrate with the historical Landsat data record and/or to supplement/enhance this record.

In this study, we develop an efficient mapping algorithm to map impervious surface for the lower Yangtze River Delta region of China from a time series of images from Landsat MSS, TM, ETM+ and more recent CBERS CCD data, spanning almost four decades. Our aim is to produce a time series of consistent impervious surface maps from these images for this rapidly urbanizing region of the world, as a precursor to a quantitative assessment of regional urbanization. Although the mapping algorithm was developed with the lower Yangtze River Delta as a case study, the approach is not location specific and can be used elsewhere with a similar set of moderate-resolution images.

2. Study area and data

Our research area is located in the lower Yangtze River Delta, China, encompassing Suzhou, Wuxi and Changzhou, which are the three major cities within the Landsat frame. The Yangtze River Delta is one of the areas with fastest economic growth since China opened its door to the world in the late 1970s. Accompanying the rapid economic development and population growth is the dramatic urbanization in the area. For example, the non-agrarian population in Suzhou city increased by about 22% from 1982 to 1985, 25% from 1985 to 1990 and 29% from 1990 to 1995. Industrialization had great impacts on small towns in this area too. Resulting from three major economic stimulus policies from the 1980s to 2000s, this area showed clear spatial and temporal urbanization patterns associated with each policy change (Ma *et al.* 2008). There were only three cities (Changzhou, Wuxi and Suzhou) in the region in the late 1970s, each of which had population well under one million. Each of these three cities has a population of several million today. In addition, there are five new cities today, each with a population above 400 000, and 205 towns, each with a population between 10 000 and 400 000 (Ma *et al.* 2008).

To detect the urban expansion in this area, we selected eight Landsat images (WRS-2 path = 119 and row = 38; central location: 120.31° E and 31.75° N) from 1973 (MSS) to 2005 (ETM+) and a CBERS image (provided free from our collaborators) in 2006 in this study (table 1). Most of the selected scenes are very clear except for the ETM+ image acquired on 26 May 2002. This ETM+ image looks hazy in the eastern part of the image. We included this hazy image to examine the robustness of the algorithm. We also included a gap-filled SLC-off ETM+ image (2005) in the time-series data set to test whether an SLC-off image would cause consistency problems for impervious surface mapping. A CBERS-2 CCD image acquired on 3 March 2006 was used to examine whether Landsat-like data could be integrated with Landsat data for change detection. Due to the proximity in time, the CBERS CCD image could be used in place of the Landsat 7 ETM+ SLC-off image to understand whether the SLC-off image (acquired a year ago on 31 March 2005) could be used for impervious surface mapping.

3. Approach

The essence of our approach is to take a time series of images from multiple sensors over a particular spatial domain as an integrative whole, thus allowing the removal of inconsistent changes. Many change detection methods for urban growth analysis

Table 1. Landsat (Lnd) and CBERS data used in this study (WGS path/row = 119/38).

Image index	Date	Satellite	Sensor	Data quality
1	16 November 1973	Lnd 1	MSS	Good
2	25 May 1979	Lnd 3	MSS	Good
3	8 May 1984	Lnd 4	MSS	Good
4	23 July 1991	Lnd 5	TM	High
5	3 August 1995	Lnd 5	TM	High
6	4 May 2000	Lnd 7	ETM+	High
7	26 May 2002	Lnd 7	ETM+	Some cloud
8	31 March 2005	Lnd 7	ETM+	Gap-filled
9	3 March 2006	CBERS	CCD	Good

process each image independently and then employ pixel-by-pixel comparison to identify land-cover/land-use changes and, thus, may suffer from the problem of error propagation in the overlay analysis (Weng and Lu 2009). A schematic outline of our processing approach is presented in figure 1.

First, remotely sensed data from different sensors were resampled, co-registered and orthorectified through the Automated Registration and Orthorectification (AROP) package developed by Gao *et al.* (2009) using an orthorectified Landset image acquired on 23 July 1991 as the base image. The AROP package can handle input images with different spatial resolutions and/or projections. It combines multiple resampling processes (e.g. reprojection, co-registration and orthorectification) into one combined process and thus reduces errors from multiple resampling (Gao *et al.* 2009). By using a common Landsat image as the base, all input moderate-resolution data including Landsat MSS and CBERS CCD data were processed to the same

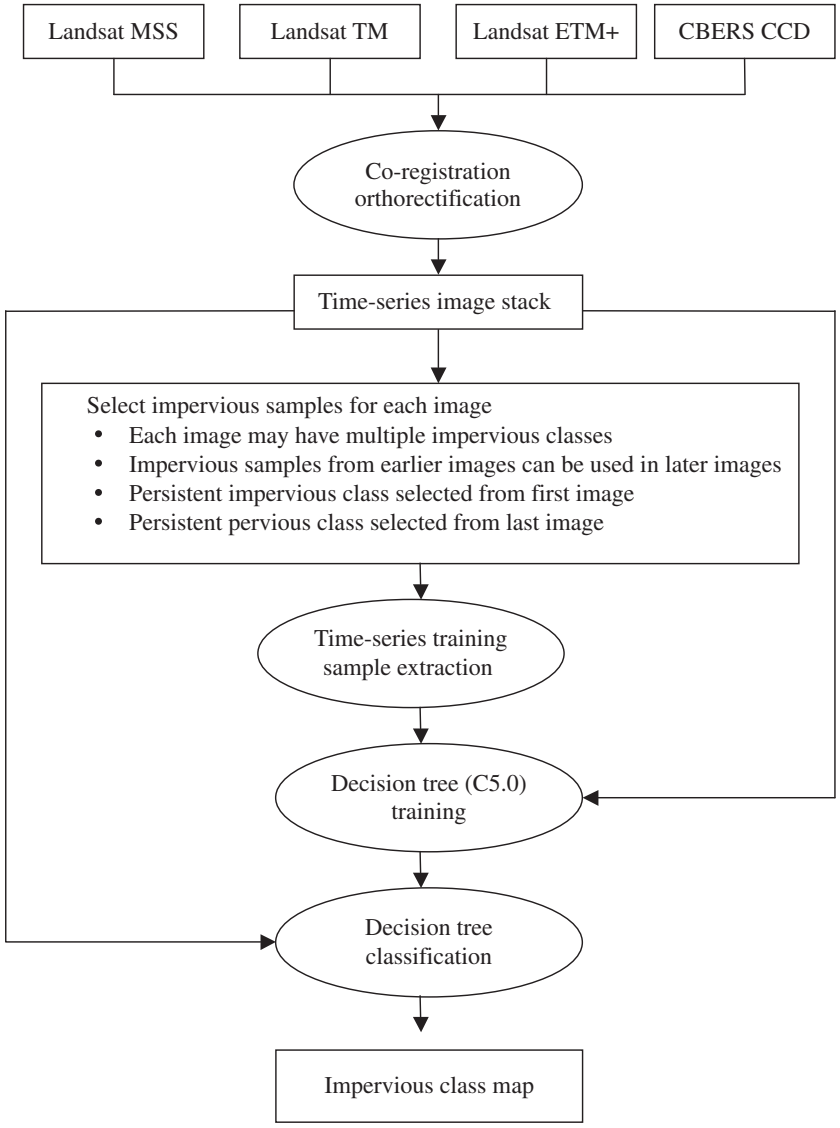

Figure 1. Processing flow chart for mapping continuous impervious surface from time-series medium-resolution remote-sensing images.

grid and spatial resolution. The input data can be in digital number, radiance, top-of-atmosphere (TOA) reflectance or atmospherically corrected surface reflectance. In this study, we calibrated MSS data to TOA reflectance. The TM and ETM+ images were processed to surface reflectance using the Landsat Ecosystem Disturbance Adaptive Processing System (LEDAPS) (Vermote *et al.* 2002, Masek *et al.* 2006). Because calibration coefficients for CBERS data were not available for this study, we used CBERS data in original digital numbers (DNs). All images in the time series were stacked into a single multi-temporal composite image before classification. Because the training data obtained from an image layer in the stack will only be used for that layer during the classification process, the unit of the remotely sensed data would not matter, nor would the units of the image layers in the stack need to be consistent as long as each layer of the training data and the corresponding layer from the image stack to be classified are on a common measurement scale (Song *et al.* 2001).

In the second step, impervious samples were selected from each image. This was done manually for each image based on visual inspection of the brightness of impervious surface. Typically, older impervious surfaces are dark in the image, whereas newer surfaces are relatively brighter. We assumed that the process of creating impervious surface was irreversible during the time of our study (i.e. the impervious surface cannot revert to the pervious state). Therefore, the impervious samples from the earlier years could be used in the later years. We selected two to eight impervious classes in different brightness levels as training samples from each image. The number of impervious classes also depended on the image quality. For example, fewer impervious classes could be selected on the MSS images because of their lower signal-to-noise ratio, and thus lower brightness contrasts among impervious classes. For each image, we focused on new impervious types, as these are not represented in the earlier images. Figure 2 shows the combined urban training samples on a subset area of the 2006 CBERS CCD image covering the city of Wuxi. Polygons delineating urban training samples in the earlier image can be used in this image for urban training data collection.

After collecting a representative set of impervious surface types for all images, we computed a normalized spectral distance (similarity) to impervious surface on a pixel-by-pixel basis for each image using the impervious surface samples from the same image. The smallest distance from all classes is computed using equations (1) and (2) and a single minimum distance map was created for each image as:

$$S_{\min} = \min_{i=1}^{n}\{s_i\}, \tag{1}$$

$$s_i = \sqrt{\frac{1}{m}\sum_{j=1}^{m}\left(\frac{x_j - \bar{x}_i}{\sigma_i}\right)^2}, \tag{2}$$

where $\bar{x}_i$ and σ_i are the mean and standard deviations of impervious type i, respectively; n is the total number of impervious classes within the image; x_j is the pixel value for band j in either DN, TOA reflectance or surface reflectance depending on the input data; and m is the number of bands. Because the impervious samples included various impervious types, such as different urban building materials, surface and illumination conditions, the minimum distance map rendered the heterogeneous impervious surface types into a simple distance map.

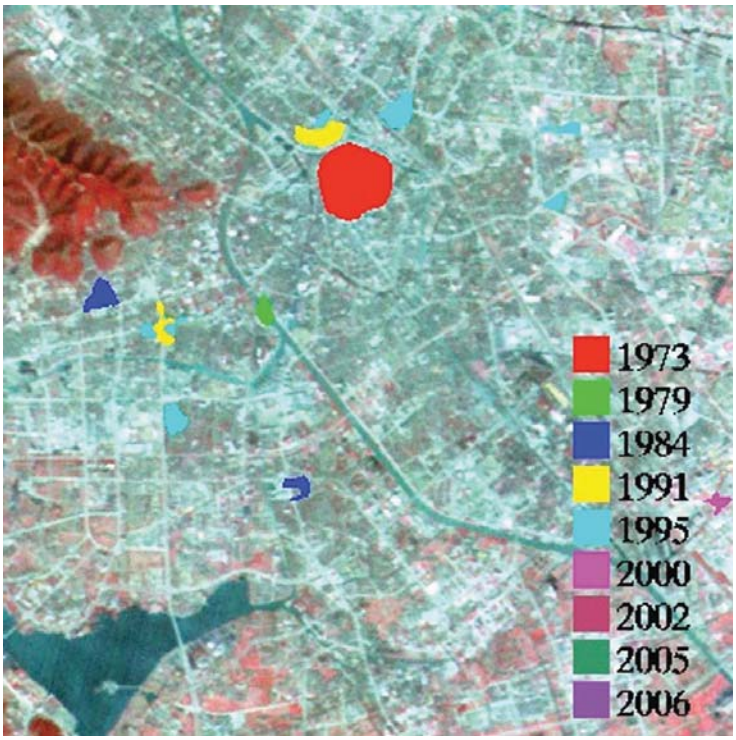

Figure 2. A subset window (the city of Wuxi centred at 31° 33′ N, 120° 18′ E) showing impervious samples selected in different years overlaid on the 2006 CBERS CCD image. Note that samples for 2002, 2005 and 2006 are too far way to be shown.

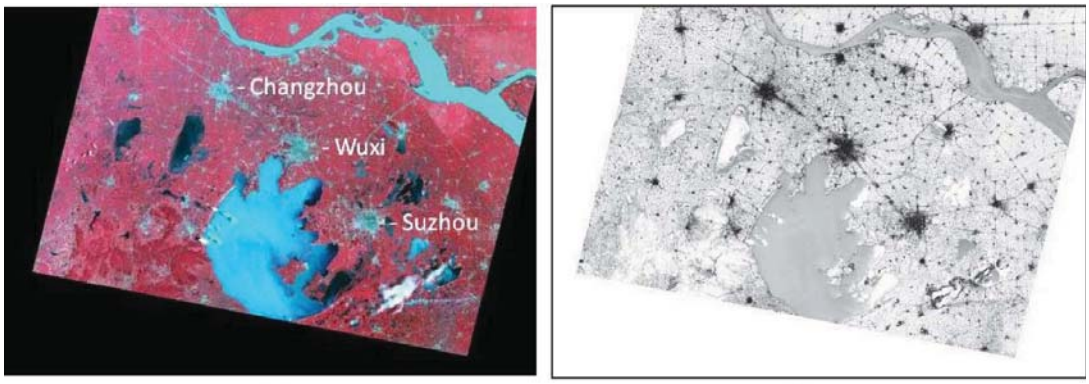

(*a*) (*b*)

Figure 3. Impervious spectral distance (similarity) map for the Landsat TM image on 3 August 1995 (the entire study area with same centre as figure 2). The darker pixels in (*b*) show shorter spectral distances to impervious samples and thus are more likely to be an impervious type. The three biggest cities in this area from northwest to southeast are Changzhou, Wuxi and Suzhou, respectively. (*a*) Landsat 5 TM, 3 August 1995 and (*b*) spectral distance to impervious samples.

Figure 3 shows an example of the spectral distance map for the Landsat 5 TM image acquired on 3 August 1995. The darker tone in figure 3(*b*) shows smaller spectral distances (i.e. higher similarity) to impervious surface. Only those samples with high confidence (either low or high spectral distance) were used as training samples. In this study, we considered pixels with $S_{\min} < 0.75$ (standard deviation) as 'confident

impervious' samples and with $S_{min} > 1.5$ (standard deviation) as 'confident pervious' samples based on our inspection of the distance image. No pixel with a distance value between 0.75 and 1.5 was included in the training set. The cloud shadows in the lower right corner in figure 3(*a*) produced small false distance values in figure 3(*b*). This issue was resolved by our subsequent time-series consistency checks. The predefined persistent pervious samples (from the most recent image) and persistent impervious samples (from the earliest image) are used in the sample training regardless of their S_{min} values.

Figure 4 shows three typical samples extracted from the time-series distance images. Figure 4(*a*) represents a persistent pervious pixel selected from the most recent image. It shows a large spectral distance at all time steps. The persistent impervious sample (figure 4*b*) selected from the earliest image shows small spectral differences in all distance images. The expanded impervious sample (figure 4(*c*)) computed from each individual image shows large spectral distance to impervious samples in the first two images, and small distance for the rest of the images in the time series, which implies the surface type changed to the impervious type during the interval between the second and the third image acquisitions.

In the third step, the time-series spectral distance maps were then stacked into a multiple layer distance image set and were used to expand impervious surface samples for classification. Based on the criteria given above, i.e. $S_{min} < 0.75$ for impervious surface and $S_{min} > 1.5$ for the pervious surface, we expanded the training samples from the distance image stack. These expanded samples would undergo an additional consistency check. Based on the irreversibility assumption, persistent impervious samples should be selected from the earliest image and should remain impervious in all images, and persistent pervious samples should be selected from the most recent image because if a pixel was pervious in the most recent image it could not be impervious in any of the previous images. For transient impervious surface, once a pixel was converted from pervious to impervious, it will remain impervious in the later images. Pixels that violate these rules would be removed from the training set. Given a set of n images, there will be a total of $(n + 1)$ classes, including a persistent impervious class, a persistent pervious class and $(n - 1)$ transient impervious classes (table 2). Therefore, we will be able to generate a single layer class map from the n-layer distance maps. Due to the conservative criteria we applied, we only have class membership for the pixels we are highly confident of, thus the expanded training samples can be used for classifying the whole image.

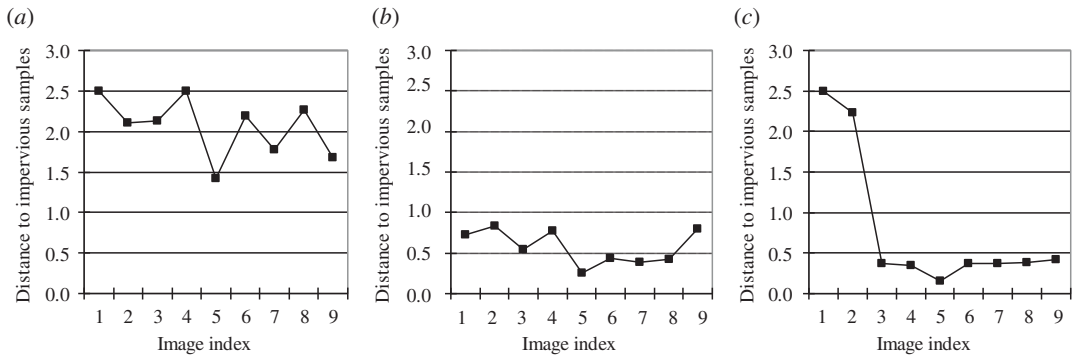

Figure 4. Temporal characteristic of changes in different impervious classes from the time-series distance images: (*a*) persistent pervious surface; (*b*) persistent impervious surface; and (*c*) expanded impervious surface.

Table 2. The complete set of impervious surface classes based on the time of change from pervious to impervious in the time-series satellite images (1 = impervious and 0 = pervious. T_i represents remote-sensing observation at time i).

Class index	T_1	T_2	T_3	. . .	T_i	. . .	T_n	Description
0	1	1	1	1	1	1	1	Persistent impervious from T_1 to T_n
1	0	1	1	1	1	1	1	Transient impervious since year T_2
2	0	0	1	1	1	1	1	Transient impervious since year T_3
. . .	0	0	0	. . .	1	1	1	. . .
$i-1$	0	0	0	0	1	1	1	Transient impervious since year T_i
. . .	0	0	0	. . .	1	1	1	. . .
$n-1$	0	0	0	0	0	0	1	Transient impervious since year T_{n-1}
n	0	0	0	0	0	0	0	Persistent pervious T_1–T_n

Once the expanded training samples were generated from the n-layer distance image stack, we will no longer need the distance maps to be stacked for classification. In the final step, the $(n + 1)$ class map would be used to train a non-parametric decision tree classifier (C5.0 by RuleQuest) on the multiple temporal composite image stack with all the images arranged in the order of time collected. Unlike traditional maximum likelihood classification, which computes class membership probability based on statistical parameters from training data assuming normal distribution of the image data, the C5.0 decision tree is a rule-based classifier. The classification rules are generated from training samples. C5.0 does not make assumptions for data distribution. The classifier has been widely used for classifying remotely sensed images, including the global land-cover product from MODIS (Friedl *et al*. 2002). An advantage of a decision tree approach is that it can handle missing values, such as gaps in non-overlapping regions. C5.0 provides several options, such as adaptive boosting, to improve classification accuracy. In this study, we chose to use the default option. The trained decision trees were then applied to the image stack for classification. The classification would result in a $(n + 1)$ class map covering the entire image frame.

4. Results and analysis

4.1 *Urban expansion in time*

Figure 5 shows a subset of different impervious classes (right column) detected from the classification, representing the approximate time period when the pervious-to-impervious change occurred. The corresponding satellite imagery (left column) for each time period is also provided for comparison. Based on visual inspection, the impervious maps on the right column generally capture impervious spatial extent well. As our process used the time-series images as a whole for training and classification, a single or a minority number of images with less than ideal image quality, such as thin cloud/hazy contamination, had a very limited effect on the results. In this study, the cloud shadows in the 1995 Landsat 5 TM image (figures 5 (*a*5) and (*b*5)) did not affect our analyses on the impervious maps for the previous (1991) and the next (2000) time periods. However, the impervious information in the thick cloudy areas of the 1995 imagery could not be detected accurately. Then clouds or hazy areas in the 2002 Landsat ETM+ (figure 5 (*a*7)) image did not show much impact on the impervious map. The incomplete image information in the 2002 image was compensated by the next (2005) or the previous (2000) clear image, indicating that users might be able

to produce a complete impervious map from a multi-temporal composite image containing multiple partially cloudy images during a relatively short acquisition period (we assume no significant change of impervious surface during this period). Gap-filled Landsat ETM+ SLC-off scenes may also be used with this approach for the same reason. Both starting and ending images are critical in determining the persistent

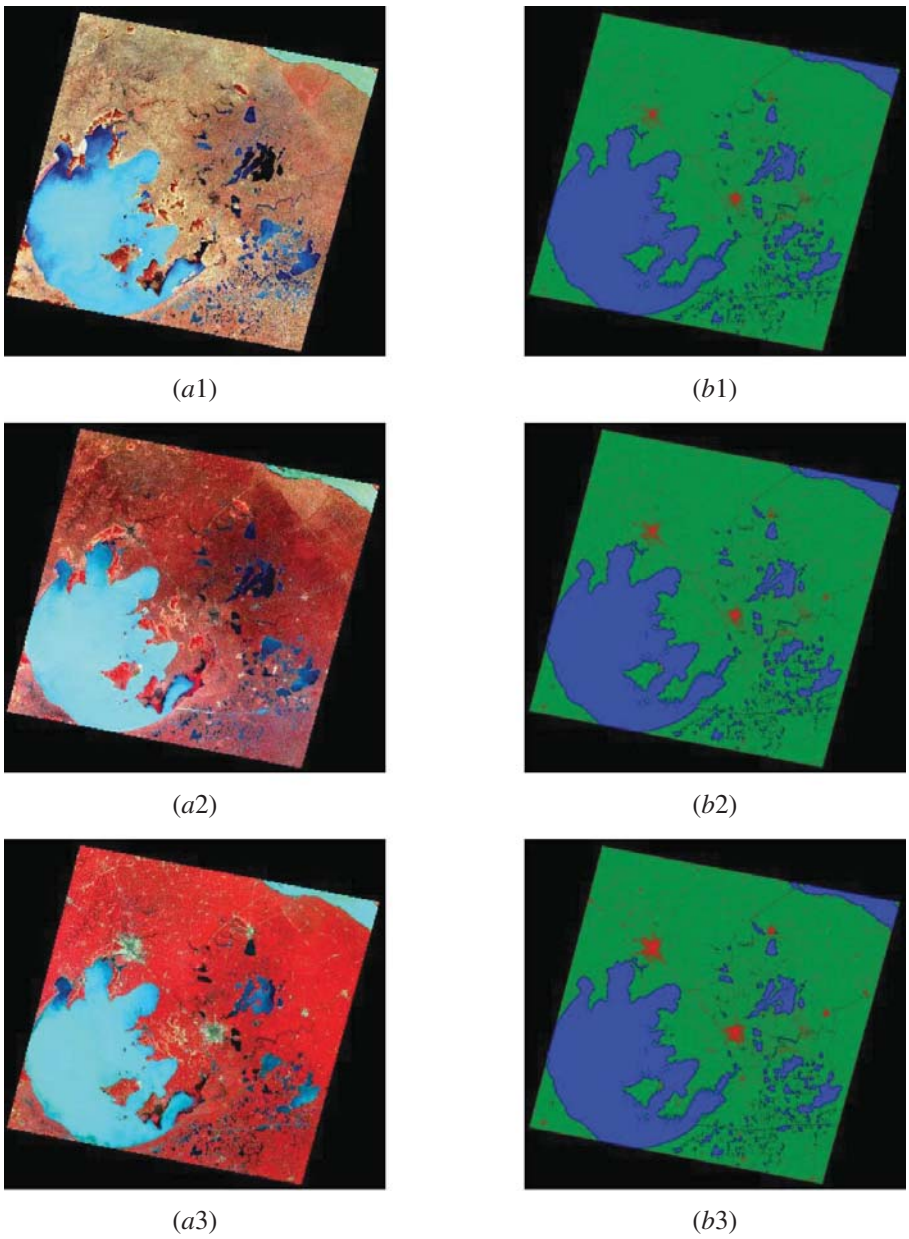

Figure 5. Time-series impervious maps (right column) as detected from Landsat or CBERS images (left column) centred at 31° 26′ N, 120° 28′ E. Colour scheme for the right column: red = impervious; green = pervious; blue = water. (*a*1) Landsat 1 MSS, 16 November 1973; (*a*2) Landsat 3 MSS, 25 May 1979; (*a*3) Landsat 4 MSS, 18 May 1984; (*a*4) Landsat 5 TM, 23 July 1991; (*a*5) Landsat 5 TM, 3 August 1995; (*a*6) Landsat 7 ETM+, 4 May 2000; (*a*7) Landsat 7 ETM+, 26 May 2002; (*a*8) Landsat 7 ETM+, 31 March 2005; and (*a*9) CBERS CCD, 3 March 2006. Time-series impervious maps detected in the years 1973 (*b*1), 1979 (*b*2), 1984 (*b*3), 1991 (*b*4), 1995 (*b*5), 2000 (*b*6), 2002 (*b*7), 2005 (*b*8) and 2006 (*b*9).

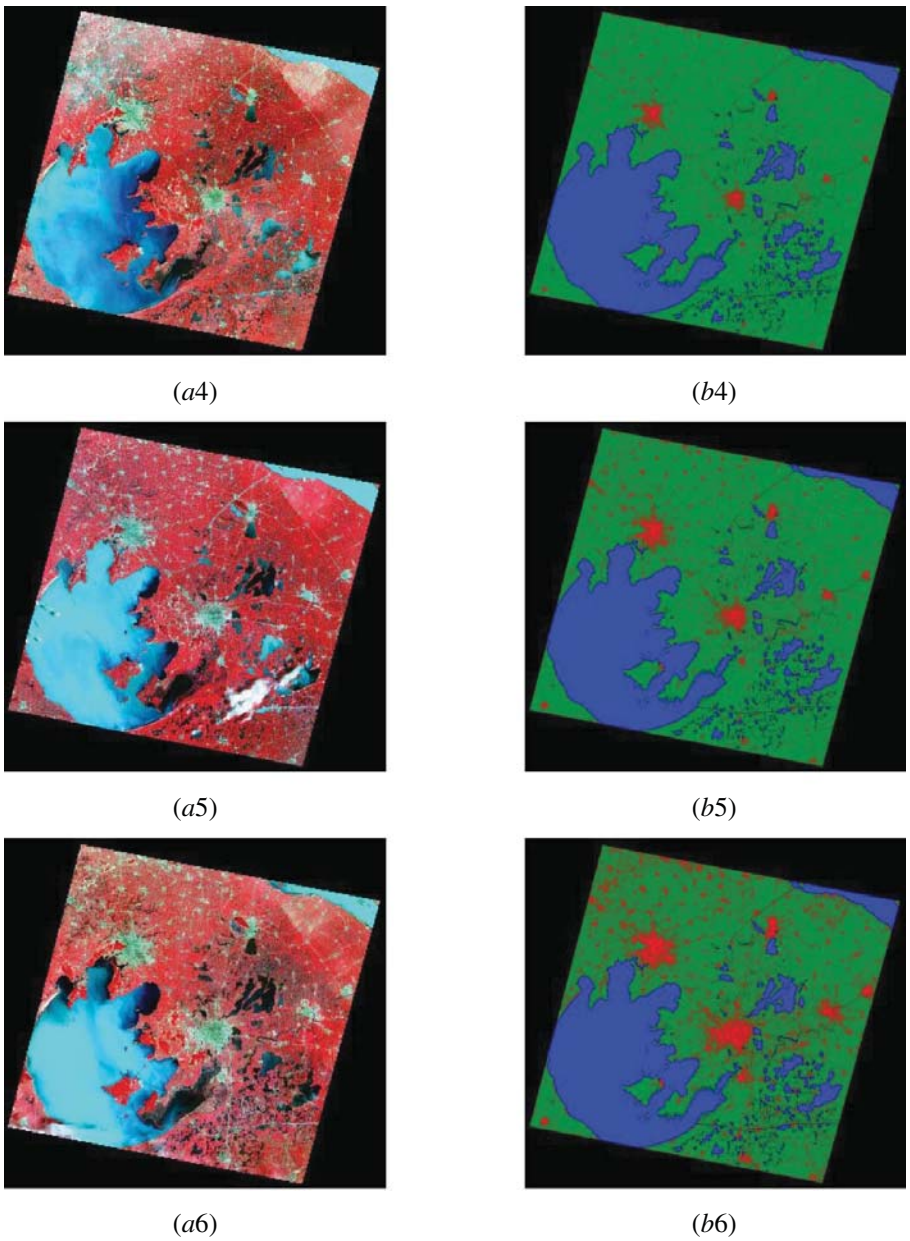

(*a*4) (*b*4)

(*a*5) (*b*5)

(*a*6) (*b*6)

Figure 5. (*Continued.*)

impervious and pervious types. In this case study, we used MSS and CBERS data as the starting and ending scenes. Figure 5 shows that results from MSS and CBERS images with different spatial resolutions are both reliable and useful and can thus be used with confidence in the continuous impervious surface mapping together with Landsat TM and ETM+ data.

The total areas of impervious surface for the common region from all input images are shown in figure 6. Results show that the impervious area in the Yangtze River Delta area increased slowly before the 1990s, started to accelerate during the 1990s and then surged from 2000 to 2006. This can also be observed from the detected impervious maps shown in figure 5. Before 1991, cities were just 'islands' and expanded slowly from town centres Between 1991 and 2000, urban expansion started to accelerate

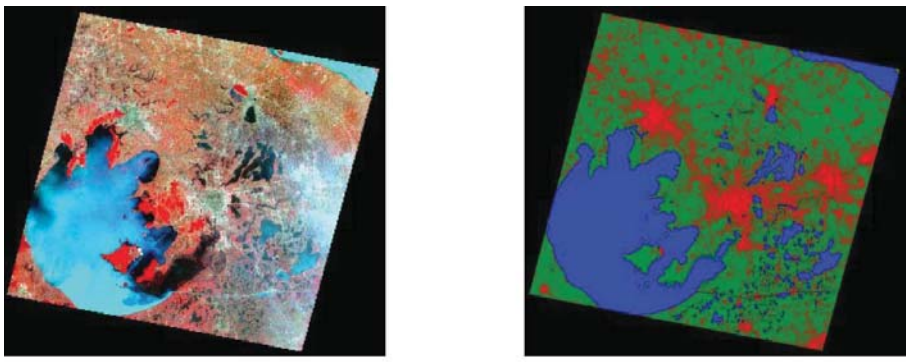

(*a*7) (*b*7)

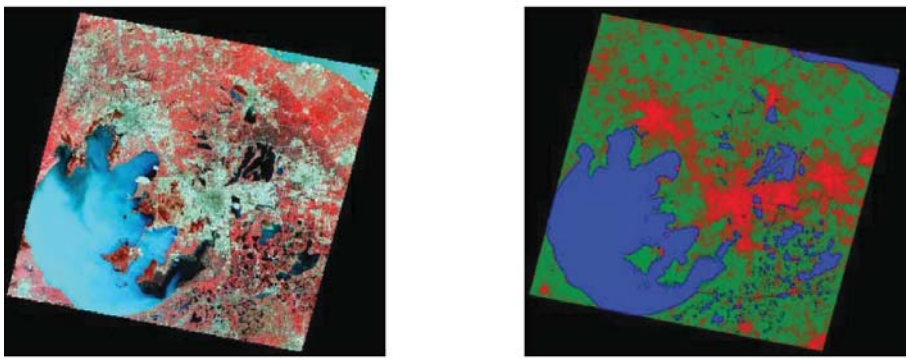

(*a*8) (*b*8)

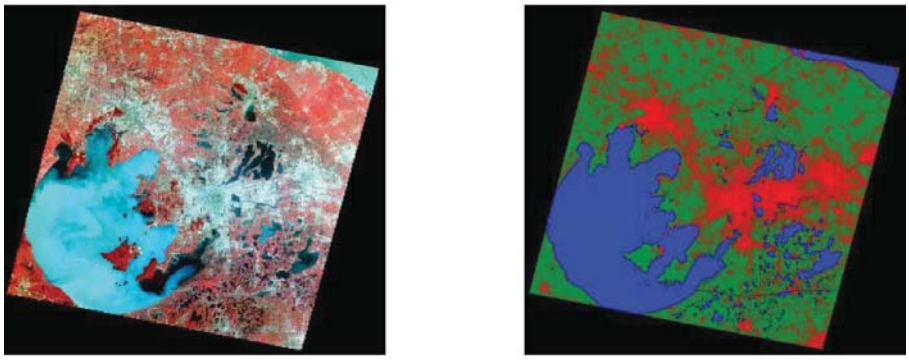

(*a*9) (*b*9)

Figure 5. (*Continued.*)

but cities were still well separated. From 2002 onwards, big cities, such as Wuxi and Suzhou, were essentially connected by new built-up areas. The pattern of impervious spatial expansion seems to follow the diffusion–coalescence model proposed by Dietzel *et al.* (2005), i.e. early-stage urban expansion occurs in isolated patches (diffusion), with further urban expansion eventually filling the gaps between the urban centres, making the previously isolated urban areas connected (coalescence). The temporal development pattern of impervious surface agrees with the urban development plan and the three stages of the national 'open door' policy in China. The first stage started in the year 1984 when China opened 14 coastal cities to serve as import/export ports to foreign countries. The Yangtze River Delta and the Pearl River Delta are the two designated special economic zones, where regional developments were limited and

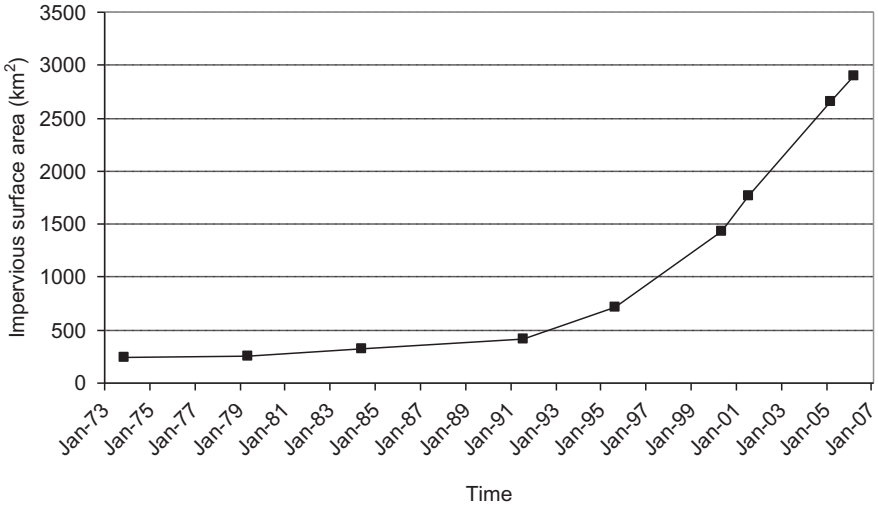

Figure 6. Temporal trajectory of total impervious surface area in the study area. The impervious surface areas before, during and after the 1990s reflect the overall economic development stages in China.

controlled by the central government. The second stage started in the year 1992 when China embraced a socialist market economy. Under this policy, the Yangtze River Delta area attracted a large amount of foreign direct investment due to its convenient location. Many towns in this area accelerated their development as a result. The third stage started in the year 2000. Large chunks of previously unconnected urban areas coalesced during 2000 to 2003, as can be clearly seen in figure 5. In this period, the industrial economy became a dominant sector in the Chinese economy. The detected areal changes of impervious types shown in figure 6 showed similar development stages.

4.2 *Urban expansion map evaluation*

Evaluating classification results of historical images is always a challenge as one cannot go back in time to collect independent ground truth. Therefore, one's ability to evaluate quality relies on the quality of existing maps that are produced either earlier or independently. In this study, we used the existing urban polygon maps produced independently by Ma *et al*. (2008). These maps were produced through visual interpretation of Landsat images. Although time consuming, visual interpretation remains one of the most accurate approaches for image classification as the interpreter can use the contextual, topological and morphological information that cannot be explicitly used with computer algorithms. Figure 7 shows that the impervious maps produced in this study agree well with urban polygons produced by Ma *et al*. (2008) based on a subset of our study area for Suzhou, the largest city in the study area. These urban polygons were visually interpreted and digitized from Landsat MSS (4 August 1984), Landsat TM (23 July 1991), Landsat ETM (4 May 2000) and IRS-P6 LIS (3 May 2005) images. The 1991 and 2000 Landsat images are in fact the same as those used in this study. Ma *et al*. (2008) defined urban polygons as residential and commercial areas, industrial and economic development zones and open space (e.g. water and green lands) if it is completely surrounded by urban land-use types. Therefore, the definitions of an urban polygon and impervious surface do not exactly match. The urban polygons show the

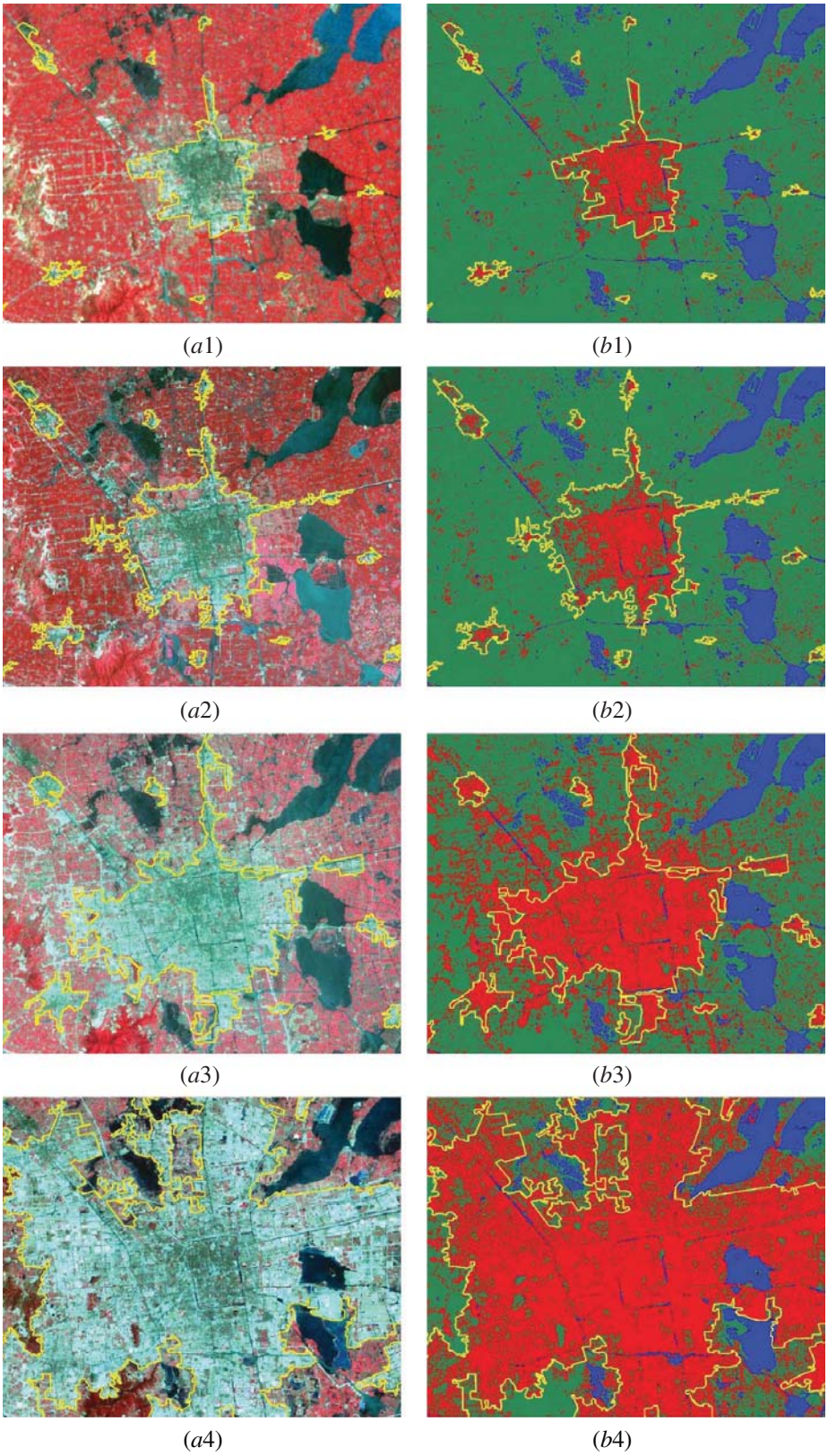

Figure 7. Urban polygons (yellow) from a previous study in Suzhou city (centred at 31° 18′ N, 120° 38′ E) (Ma *et al.* 2008) overlaid on the original image (left) compared with the same polygons overlaid on the impervious maps (right) detected from time-series images in this study. (*a*1) Landsat 4 MSS, 8 May 1984; (*a*2) Landsat 5 TM, 23 July 1991; (*a*3) Landsat 7 ETM+, 4 May 2000; and Landsat 7 ETM+, 31 March 2005. Polygons overlaid on the impervious maps detected on 4 August 1984 (*b*1), 23 July 1991 (*b*2), 4 May 2000 (*b*3) and 3 May 2005 (*b*4).

extent of the urban/city as a whole object, whereas our impervious maps only show impervious/built-up types at the pixel scale, and with potentially more spatial detail. Some discrepancies can be found between urban polygons and impervious maps due to their different definitions. The 1991 impervious map (figure 6 (*b*2)) shows smaller detected impervious areas than urban polygons. The urban polygons are somewhat extended to include new industrial development areas in the suburb of Suzhou City, while the 1991 Landsat TM image (figure 6 (*a*2)) still shows strong vegetation signals in these suburb areas.

Table 3 shows the overall accuracies for both impervious and pervious classes. The evaluation samples were selected from each individual image randomly. For each image, we selected about 600–700 pixels for accuracy assessment. The urban polygons in the reference data were used as the basic sampling unit. The impervious types include various bright (new) and dark (old) objects or areas. The pervious types are mostly located in suburban areas. As samples are purely based on the visual interpretation of images at the same resolution, the accuracy assessments should not be over interpreted. We are more interested in examining the capability of the algorithm and tended to select evaluation samples that are hard to distinguish. The overall accuracies may be better than what table 3 shows if areas of crops and water are included proportionally in the accuracy assessment. The overall accuracies vary in different years from 87% to 98%.

A combined classification error matrix is shown in table 4. This includes assessment from all input images, including MSS, TM, ETM+ and CBERS. The omission error for the impervious type is about 12.2%. The commission error for the impervious type is about 2.7%. The larger omission error may partially be due to the sample selection approach (polygon-based). A pixel-based sample selection approach would be more appropriate for accuracy assessment as evaluation sample polygons usually contain some pervious pixels such as rivers and parks. Due to the lack of a time series of high-resolution satellite images or aerial photos, we cannot provide as rigorous an accuracy assessment in our study as one would prefer. Considering our assessments are based on inputs from different spatial resolution images with different image qualities, the results are quite promising. We expect the algorithm to perform better if a data set

Table 3. Overall classification accuracies for different years.

Year	1973	1979	1984	1991	1995	2000	2002	2005	2006
Accuracy (%)	88.0	87.3	95.4	94.3	94.7	98.1	89.9	90.8	93.7

Table 4. Combined classification error matrix from all images listed in table 1.

Pixels and percent	Classification results		Producer's accuracy	Omission errors
	Impervious	Pervious		
Reference data				
Impervious	5324	741	87.8%	12.2%
Pervious	157	5710	97.3%	2.7%
User's accuracy	97.1%	88.5%		
Commission errors	2.9%	11.5%		92.5%

consisted of more consistent images, such as images from a single sensor (e.g. Landsat TM) so that there is less noise from variation in spatial resolution and no variation in spectral separablility for the same classes across image layers.

5. Discussion

In this article, we successfully used remotely sensed data from four sensors with different spatial resolutions to produce a consistent impervious surface map over several decades. We resampled both MSS and CBERS images to 30 m × 30 m spatial resolution to match with that of TM/ETM+ data. Results show that Landsat MSS images are acceptable in extending the time series of images for mapping impervious surface expansion.

We noted that the algorithm does not address pixels that are partially urbanized. Although the 30 m × 30 m spatial resolution impervious product is much more accurate at local and regional scales compared with the 1 km × 1 km global products and is produced at a high temporal resolution from mixed data streams, there are still mixed pixels at this spatial resolution. In fact, mixed pixels exist regardless of what the spatial resolution is because the natural world features are predominantly continuous, and typically not organized as regular grids. A possible alternative solution is to extract subpixel impervious fractions (Wu and Murray 2003, Song 2005) for the analysis. The choice between a discrete classification and a subpixel fraction method depends on the scale and application.

A possible drawback in using 30 m × 30 m spatial resolution data for change detection is its sensitivity to the co-registration accuracy for images obtained from different sensors or the same sensor at different times. The location shifts due to image-to-image registration errors may cause spurious changes. This problem will be particularly serious at the edges or with linear impervious features. Image classification based on the time-series image stacks requires very accurate location registration at the sub-pixel level. Our checking process for consistent impervious areas can preserve high-quality time-series training samples and reduce errors from mis-registration or other sources of noise.

Mapping time series of impervious cover at a coarser resolution (e.g. 60 m) may be able to produce higher mapping accuracies (less noisy), but a coarser spatial resolution will suffer more from the problem of mixed pixels.

Despite the sensitivity to registration error, the algorithm developed in this study that treats multi-temporal images as an integrative whole does offer several significant advantages. First, it enables the capability to remove inconsistent changes. Not all impervious pixels remain completely static. Some impervious pixels may appear vegetated such as trees planted along newly built roads and parking lots or on roof tops. However, these superficial changes do not alter the fundamental property of the imperviousness underneath the vegetation, although urban vegetation does provide other benefits, such as relief of surface urban heat island effects (Li *et al*. 2011). These types of pixels can be extremely difficult to account for in conventional classifications using a single image. The irreversibility assumption for the imperious surface suppressed this type of noise. Second, the algorithm is robust to image noise. The images we used in this study are from different seasons. The seasonal variation in sun angle, phenology and surface wetness would pose a major challenge to a conventional classification approach. These types of errors have no effect in the algorithm we developed here because the training samples were selected based on relative similarity

scores, and the classification was performed on a whole set of images as if it were a single multiple band image. Finally, our approach does not require data normalization (e.g. conversion to reflectance or other physical units). Data normalization is a huge task in conventional land-cover/land-use classification and change detection applications (Song *et al*. 2001). Our algorithm makes normalization unnecessary for the same reasons as given above.

As this is a supervised classification approach, the classification results depend on the quality of training samples. Figure 8 shows the combined time-series impervious year and the associated confidence map produced from the same C5.0 decision tree classifier. The map shows high confidence over pervious classes such as water and croplands, and lower confidence (<50%, in red) on some impervious areas in the eastern suburb of Suzhou. This may be due to the low-quality image (thin cloud/hazy in the 2002 image) in this area. The classification can be improved by using high-quality images or through an iterative selection on impervious and pervious samples on those less confident areas.

Further validation using different data sources such as high-resolution satellite images or aerial photos from various years can give a more precise assessment on the classification accuracies. It is always a challenge to validate classification results even for single image classification. In the future, we plan to focus on other rapidly urbanizing areas with more extensive high-resolution satellite images or aerial photos for algorithm testing and validation. There are now rich sources of moderate-resolution remotely sensed data that allow us to move from more regional to continental, and even global scales to map urbanization (Gutman *et al*. 2008). Significant challenges remain for mapping urbanization over large areas, in terms of not only validation but also systematically processing data from multiple time periods, sources/instruments and seasons. Our algorithm shows a path forward.

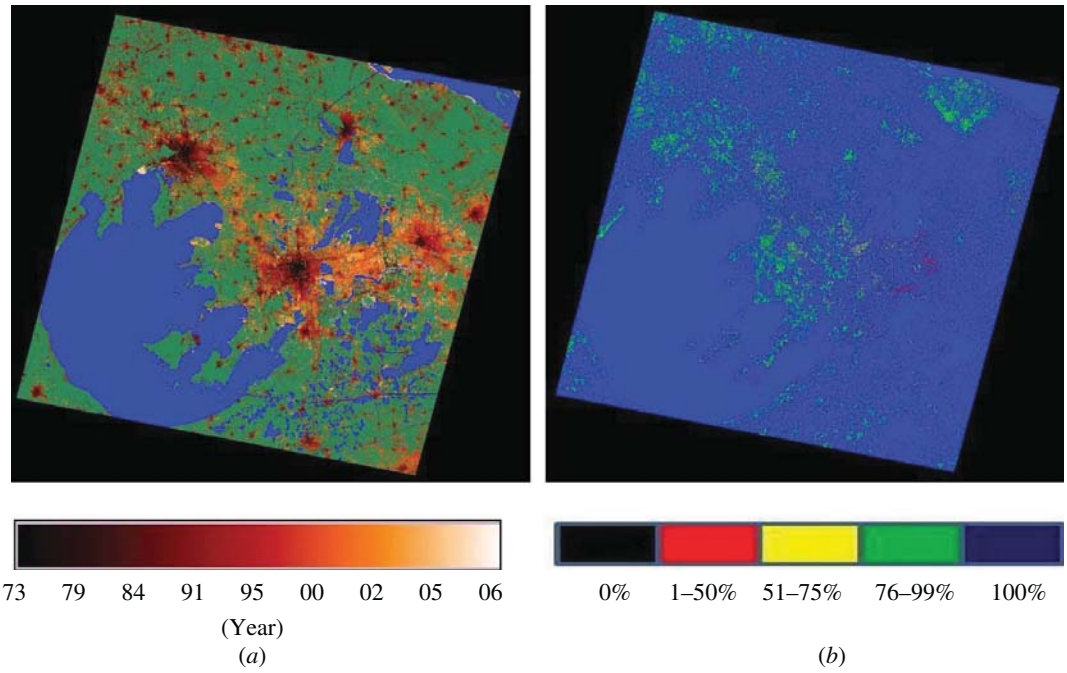

Figure 8. Urban expansion map (*a*) and the associated confidence maps (*b*) may be used to assess the classification results and to improve time series by selecting more impervious or pervious samples in the less confident areas.

6. Conclusion

This article developed a new algorithm to map the continuous urban expansion process from time series of satellite images. The algorithm produced urban expansion maps of the lower Yangtze River Delta area of China with high accuracy when compared with an independent data set. The algorithm included remotely sensed data from different sources and spatial resolutions, including Landsat MSS, TM/ETM+ and data from CBERS. Because the multitemporal images were treated as an integrative whole, no noise removal or calibration was needed. The approach effectively integrated Landsat TM and ETM+ data with other imagery in monitoring urban expansion and showed a strong potential to extend the satellite data record for land-cover/land-use change detection.

Clouds and their shadows were shown to have minor effects on the change analysis. The partially cloudy or gap-filled images were also shown to be useful for the time-series analysis using our approach, significantly simplifying the image-processing efforts. This algorithm can easily be adapted to other remote-sensing data sources and extended to other regions. As Landsat data are currently freely available, it is now possible to produce regional, continental or global time-series impervious maps from historical Landsat or Landsat-like data. Although significant challenges remain in effectively and consistently processing a global time series of medium-resolution data, time-series impervious cover maps can provide an improved and more detailed data source to evaluate the impact of the urbanization process on the environment as well as any potential effects on climate change.

Acknowledgements

This work was supported by the US Geological Survey (USGS) Landsat Science Team project, the NASA Land Cover and Land Use Change (LCLUC) project and the Strategic Priority Research Programme of the Chinese Academy of Sciences, Climate Change: Carbon Budget and Relevant Issues, Grant No. XDA05050106.

References

Dietzel, C., Oguz, H., Hemphill, J.J., Clarke, K.C. and Gzaulis, N., 2005, Diffusion and coalescence of Houston Metropolitan Area: evidence supporting a new urban theory. *Environment and Planning B – Planning and Design*, **32**, pp. 231–246.

Elvidge, C.D., Baugh, K.E., Kihn, E.A., Kroehl, H.W. and Davis, E.R., 1997, Mapping city lights with nighttime data from the DMSP Operational Linescan System. *Photogrammetric Engineering and Remote Sensing*, **63**, pp. 727–734.

Friedl, M.A., McIver, D.K., Hodges, J.C.F., Zhang, X., Muchoney, D., Strahler, A.H., Woodcock, C.E., Gopal, S., Schneider, A., Cooper, A., Baccini, A., Gao, F. and Schaaf, C., 2002, Global land cover from MODIS: algorithms and early results. *Remote Sensing of Environment*, **83**, pp. 135–148.

Gao, F., Masek, J. and Wolfe, R., 2009, An automated registration and orthorectification package for Landsat and Landsat-like data processing. *Journal of Applied Remote Sensing*, **3**, 033515, doi:10.1117/1.3104620.

Grimm, N.B., Faeth, S.H., Golubiewski, N.E., Redman, C.L., Wu, J., Bai, X. and Briggs, J.M., 2008, Global change and the ecology of cities. *Science*, **319**, pp. 756–760.

Groffman, P.M., Bain, D.J., Band, L.E., Belt, K.T., Brush, G.S., Grove, J.M., Pouyat, R.V., Yesilonis, I.C. and Zipperer, W.C., 2003, Down by the riverside: urban riparian ecology. *Frontiers in Ecology and the Environment*, **1**, pp. 315–321.

Gutman, G., Byrnes, R., Masek, J., Covington, S., Justice, C., Franks, S. and Headley, R., 2008, Towards monitoring land-cover and land-use changes at a global scale: the global land survey 2005. *Photogrammetric Engineering and Remote Sensing*, **74**, pp. 6–10.

Gutman, G., Janetos, A.C., Justice, C.O., Moran, E.F., Mustard, J.F., Rindfuss, R.R., Skole, D., Turner II, B.L. and Cochrane, M.A., 2004, *Land Change Science: Observing, Monitoring and Understanding Trajectories of Change on the Earth's Surface*, 457 p. (Dordrecht: Kluwer Academic Publishers).

Herold, M., Goldstein, N.C. and Clarke, K.C., 2003, The spatialtemporal form of urban growth: measurement, analysis and modeling. *Remote Sensing of Environment*, **86**, pp. 286–302.

Homer, C., Huang, C., Yang, L., Wylie, B. and Coan, M., 2004, Development of a 2001 national landcover database for the United States. *Photogrammetric Engineering and Remote Sensing*, **70**, pp. 829–840.

Imhoff, M.L., Lawrence, W.T., Stutzer, D.C. and Elvidge, C.D., 1997, A technique for using composite DMSP/OLS 'city lights' satellite data to map urban areas. *Remote Sensing of Environment*, **61**, pp. 361–370.

Jantz, P., Goetz, S. and Jantz, C., 2005, Urbanization and the loss of resource lands in the Chesapeake Bay Watershed. *Environmental Management*, **36**, pp. 808–825.

Ji, C.Y., Liu, Q., Sun, D., Wang, S., Lin, P. and Li, X., 2001, Monitoring urban expansion with remote sensing in China. *International Journal of Remote Sensing*, **22**, pp. 1441–1455.

Kalnay, E. and Cai, M., 2003, Impact of urbanization and land-use change on climate. *Nature*, **423**, pp. 528–531.

Li, J., Song, C., Cao, L., Zhu, F., Meng, X. and Wu, J., 2011, Impacts of landscape structure on surface urban heat islands: a case study of Shanghai, China. *Remote Sensing of Environment*, **115**, pp. 3249–3263.

Liu, J., Tian, H., Liu, M., Zhuang, D., Melillo, J.M. and Zhang, Z., 2005, China's changing landscape during the 1990s: large-scale land transformations estimated with satellite data. *Geophysical Research Letters*, **32**, L02405, doi:10.1029/2004GL021649.

Loveland, T.R. and Shaw, D.M., 1996, Multi-resolution land characterization: building collaborative partnerships. In *GAP Analysis: A Landscape Approach to Biodiversity Planning*, J.M. Scott, T.H. Tear and F.W. Davis (Eds.), pp. 79–85 (Bethesda, MD: American Society for photogrammetry and Remote Sensing).

Ma, R., Gu, C., Pu, Y. and Ma, X., 2008, Mining the urban sprawl pattern: a case study on Sunan, China. *Sensors*, **8**, 6371–6395.

Masek, J.G., Vermote, E.F., Saleous, N.E., Wolfe, R., Hall, F.G., Huemmrich, F., Gao, F., Kutler, J. and Lim, T.K., 2006, A Landsat surface reflectance data set for North America, 1990–2000. *IEEE Geoscience and Remote Sensing Letters*, **3**, pp. 69–72.

McKinney, M.L., 2002, Urbanization, biodiversity, and conservation. *Bioscience*, **52**, pp. 883–890.

Netzband, M., Stefanov, W.L. and Redman, C., 2007, *Applied Remote Sensing for Urban Planning, Governance and Sustainability* (Berlin: Springer).

Peng, X., 2011, China's demographic history and future challenges. *Science*, **333**, pp. 581–587.

Schneider, A., Friedl, M.A., McIver, D.K. and Woodcock, C.E., 2003, Mapping urban areas by fusing multiple sources of coarse resolution remotely sensed data. *Photogrammetric Engineering and Remote Sensing*, **69**, pp. 1377–1386.

Schneider, A., Seto, K.C. and Webster, D.R., 2005, Urban growth in Chengdu, Western China: application of remote sensing to assess planning and policy outcomes. *Environment and Planning & Design*, **32**, pp. 323–345.

Seto, K.C., Kaufman, R. and Woodcock, C.E., 2000, Landsat reveals China's farmland reserves, but they're vanishing fast. *Nature*, **406**, p. 121.

Seto, K.C., Sanchez-Rodriguez, R. and Fragkias, M., 2010, The new geography of contemporary urbanization and the environment. *Annual Review of Environment and Resources*, **35**, pp. 167–194.

Seto, K.C., Woodcock, C.E., Song, C., Huang, X., Kaufmann, R.K. and Lu, J., 2002, Measuring land use change with Landsat TM: evidence from Pearl River Delta. *International Journal of Remote Sensing*, **23**, pp. 1985–2004.

Sausen, T.M., 2001, The China–Brazil Earth Resources Satellite (CBERS). *International Society for Photogrammetry and Remote Sensing (ISPRS) Society*, **6**, pp. 27–28.

Small, C., 2003, High spatial resolution spectral mixture analysis of urban reflectance. *Remote Sensing of Environment*, **88**, pp. 170–186.

Song, C., 2005, Spectral mixture analysis for subpixel vegetation fractions: how to incorporate endmember variabilities? *Remote Sensing of Environment*, **95**, pp. 248–263.

Song, C., Woodcock, C.E., Seto, K.C., Pax-Lenney, M. and Macomber, S.A., 2001, Classification and change detection using Landsat TM data: when and how to correct atmospheric effects? *Remote Sensing of Environment*, **75**, pp. 230–244.

Townshend, J., Justice, C., LI, W.., Gurney, C. and McManus, J., 1991, Global land cover classification by remote sensing: present capabilities and future possibilities. *Remote Sensing of Environment*, **35**, pp. 243–255.

United Nations, 2008, *World Urbanization Prospects: The 2007 Revision* (New York: United Nations).

Vermote, E.F., ElSaleous, N. and Justice, C., 2002, Atmospheric correction of the MODIS data in the visible to middle infrared: first results. *Remote Sensing of Environment*, **83**, pp. 97–111.

Wang, H., Wang, S., MA, W. and HE, T., 2000, Development and operation of the IRMSS and CCD camera for CBERS. In *Proceedings SPIE Infrared Technology and Applications XXVI*, Bjorn F. Andresen, Gabor F. Fulop and Marija Strojnik (Eds.) (Bellingham, WA: SPIE), vol. 4130, pp. 9–12.

Weng, Q. and Lu, D., 2009, Landscape as a continuum: an examination of the urban landscape structures and dynamics of Indianapolis city, 1991–2000. *International Journal of Remote Sensing*, **30**, pp. 2547–2577.

Woodcock, C.E., Allen, R., Anderson, M., Belward, A., Bindschadler, R., Cohen, W., Gao, F., Goward, S.N., Helder, D., Helmer, E., Nemani, R., Oreopoulos, L., Schott, J., Thenkabail, P.S., Vermote, E.F., Vogelmann, J., Wulder, M.A. and Wynne, R., 2008, Free access to Landsat imagery. *Science*, **320**, p. 1011.

Wu, C. and Murray, A.T., 2003, Estimating impervious surface distribution by spectral mixture analysis. *Remote Sensing of Environment*, **84**, pp. 493–505.

Zhou, L., Dickinson, R.E., Tian, Y., Fang, J., Li, Q., Kaufmann, R.K., Tucker, C.J. and Myneni, R.B., 2004, Evidence for a significant urbanization effect on climate in China, *Proceedings of the National Academy of Sciences of the United States of America*, **101**, pp. 9540–9544.